RESEARCH ARTICLE

Addition of sodium malonate alters the morphology and increases the critical flux during tangential flow filtration of precipitated immunoglobulins

Ali Behboudi | **Mirko Minervini** | **Zachary S. Badinger** | **William W. Haddad** | **Andrew L. Zydney** (ORCID)

Department of Chemical Engineering, The Pennsylvania State University, University Park, Pennsylvania, USA

Correspondence
Andrew L. Zydney and Ali Behboudi, Department of Chemical Engineering, The Pennsylvania State University, University Park, PA 16802, USA.
Email: zydney@engr.psu.edu and aub793@psu.edu

Abstract

Recent studies have demonstrated that one can control the packing density, and in turn the filterability, of protein precipitates by changing the pH and buffer composition of the precipitating solution to increase the structure/order within the precipitate. The objective of this study was to examine the effect of sodium malonate, which is known to enhance protein crystallizability, on the morphology of immunoglobulin precipitates formed using a combination of $ZnCl_2$ and polyethylene glycol. The addition of sodium malonate significantly stabilized the precipitate particles as shown by an increase in melting temperature, as determined by differential scanning calorimetry, and an increase in the enthalpy of interaction, as determined by isothermal titration calorimetry. The sodium malonate also increased the selectivity of the precipitation, significantly reducing the coprecipitation of DNA from a clarified cell culture fluid. The resulting precipitate had a greater packing density and improved filterability, enabling continuous tangential flow filtration with minimal membrane fouling relative to precipitates formed under otherwise identical conditions but in the absence of sodium malonate. These results provide important insights into strategies for controlling precipitate morphology to enhance the performance of precipitation-filtration processes for the purification of therapeutic proteins.

Reviewing Editor: Aitziber L. Cortajarena

1 | INTRODUCTION

Precipitation has been the dominant platform for plasma protein separations since the development of the Cohn fractionation process in the 1940s (Cohn et al., 1946; Foster et al., 1986). A number of recent investigations have demonstrated that precipitation can also be used for the purification of monoclonal antibodies (mAbs) (Dutra et al., 2020; Ferreira-Faria et al., 2023; Li et al., 2019; Pons Royo et al., 2023; Recanati et al., 2023; Recanati et al., 2024), exploiting the relatively high titers of current Chinese hamster ovary (CHO) cell cultures (Liang et al., 2023; Shukla et al., 2017). The precipitated protein can be effectively dewatered and washed using tangential flow filtration (TFF), potentially providing a low-cost platform for the continuous downstream processing of mAbs (Li et al., 2019; Minervini et al., 2023).

Recent work by Minervini et al. (2024) demonstrated that it is possible to alter the morphology of precipitated immunoglobulin G (IgG) by changing the pH, ionic strength, and specific salt composition of the solution, enabling significant improvements in the filterability of the resulting precipitate. The critical flux, that is, the highest filtrate flux at which membrane fouling remains negligible, for precipitates formed under different conditions was very well correlated with the packing density of the precipitate (determined by batch centrifugation). The highest packing density, and thus the largest critical flux, was obtained by performing the precipitation using 10 mM $ZnCl_2$ and 7 weight/volume (w/v) percent polyethylene glycol (PEG) in the presence of 300 mM $CaCl_2$, with only slightly lower performance obtained using 300 mM Na_2SO_4. The improved morphology of the protein precipitate was due, at least in part, to the slower precipitation kinetics under these conditions.

There is extensive literature on the effects of different salts on protein precipitation and the underlying physics controlling the "salting out" phenomena (Dumetz et al., 2007; Melander and Horváth, 1977; Shih et al., 1992). High salt concentrations shield intermolecular repulsive electrostatic interactions, thus decreasing the protein solubility. However, it is unclear how these changes in solubility affect the morphology of the precipitate or its packing density, which appears to be the dominant factor controlling the filterability of the precipitated protein. Instead, it is likely that the increase in packing density arises from the presence of increased order within the precipitate, suggesting that conditions that enhance protein crystallizability might also improve the filterability of the precipitate.

McPherson (2001) examined the effects of 12 different salts on the crystallization of 23 proteins including three mAbs, two chimeric antibodies (human–simian) and one mouse-derived antibody. Nineteen of the 23 proteins were successfully crystallized using sodium malonate; the next most effective salt was only able to crystallize 10 of the proteins. All three antibodies (two IgG1 antibodies and one IgG4) could be crystallized out of sodium malonate solutions; the only other salt that was able to crystallize these antibodies was sodium acetate. In addition, malonate was effective at forming protein crystals at much lower concentrations than the other salts, in some cases by as much as a factor of 10. The excellent performance of sodium malonate was attributed to its relatively high charge density (two negatively charged carboxylic acids at neutral pH) and its action as a kosmotrope in stabilizing the protein structure even at low concentrations (Collins, 1995; Collins and Washabaugh, 1985; Kaushik and Bhat, 1999). Sodium malonate is also known to stabilize previously formed protein crystals by acting as a cryoprotectant (Holyoak et al., 2003).

The objective of this study was to examine the effect of sodium malonate on the precipitation of human serum immunoglobulin G (hIgG), which is of interest in immunoglobulin therapy and as a model for the behavior of mAbs. Data were obtained for the precipitation yield as a function of $ZnCl_2$ and PEG concentrations, both in the presence and absence of sodium malonate, with the structure and morphology of the precipitate examined using differential scanning calorimetry, isothermal titration calorimetry (ITC), and bright field microscopy. The critical flux was evaluated using flux-stepping experiments, with the data demonstrating a significant improvement in filterability upon the addition of sodium malonate.

2 | MATERIALS AND METHODS

2.1 | Materials

Lyophilized human serum IgG powder was obtained from Nova Biologics (Oceanside, CA) and stored at 4°C until use. MES (2-morpholinoethanesulfonic acid) with a pK_a of 6.15 was purchased from Thermo Fisher Scientific

(Waltham, MA). Zinc chloride solutions ($ZnCl_2$, 0.1 M), PEG ($Mn \approx 3350$ Da), dibasic sodium malonate (DSM, $\geq 97.0\%$), $CaCl_2$, and Na_2SO_4 were all obtained from Sigma-Aldrich. HCl and glycine, also obtained from Sigma-Aldrich, were used for pH adjustment and precipitate redissolution, respectively.

Filtration was performed using MidiKros® polyethersulfone hollow fiber membranes (0.2 μm pore size, 1 mm ID) from Repligen Corporation (Rancho Dominguez, CA). Modules had a total membrane area of 88 cm^2 and an effective fiber length of 20 cm. Membranes were cleaned with 0.5 M NaOH at 35–40°C for at least 30 min after each experiment and then stored in 0.1 M NaOH between uses.

2.2 | IgG precipitation

IgG precipitation was performed using $ZnCl_2$ as a cross-linking agent and PEG as a volume exclusion agent based on recent results showing the selective precipitation of both IgG and mAbs using this system (Burgstaller et al., 2019; Minervini et al., 2023). The effect of sodium malonate on the precipitation yield was examined in small-scale batch precipitation experiments. IgG was dissolved in 50 mM MES buffer at pH 6.4 at a concentration of 10 g/L in the presence of different concentrations of sodium malonate, $CaCl_2$, or Na_2SO_4; 5 mL of the IgG solution was added to 5 mL of a second solution containing target levels of $ZnCl_2$ and PEG in 50 mM MES buffer at pH 6.4 to initiate precipitation. The resulting suspension was allowed to equilibrate at 4°C for 12 h. The solid precipitate was collected by centrifugation at 8000 rpm and 4°C using an Eppendorf 5415 R centrifuge. The supernatant was carefully removed, and the pellet was redissolved by the addition of 1 mL of a 2 M glycine solution. The IgG concentrations in the supernatant (S) and redissolved precipitate (R) were evaluated using an Infinite® m200 Pro microplate reader (Tecan Trading AG, Switzerland) based on the absorbance at 280 nm, with the precipitate yield calculated as:

$$Y = \frac{C_R V_R}{C_R V_R + C_S V_S}, \tag{1}$$

where C and V are the IgG concentrations and solution volumes, respectively.

Larger scale IgG precipitation was performed in a continuous tubular flow reactor fitted with static mixers (Koflo Corporation, Cary, IL) providing a total length of 70 cm. The IgG solution, at a concentration of 10 g/L, was introduced into the reactor at a rate of 5 mL/min. It was then mixed with a stream of 0.1 M $ZnCl_2$ flowing at

a rate of 1 mL/min using a Y-connector located at the entrance to the first static mixer. Simultaneously, a PEG solution with a concentration of 17.5 w/v% was added at a flow rate of 4 mL/min through a similar connector located at the entrance of the second static mixer. This process resulted in a final solution containing precipitated IgG with a concentration of 5 g/L, $ZnCl_2$ with a concentration of 10 mM, and PEG with a concentration of 7.5 w/v%. The total residence time in the tubular flow reactor was 120 s. Additional details on the continuous precipitation are provided elsewhere (Minervini et al., 2024).

The packing density (ϕ_p) of the protein precipitate was evaluated directly from the mass of the centrifuged pellet, which was calculated from the weight of the centrifuge tube with the pellet (after removal of the supernatant) minus that of the empty centrifuge tube as discussed by Minervini et al. (2024):

$$\phi_p = \frac{m_{IgG}}{m_{pellet}}, \tag{2}$$

where m_{IgG} is the total mass of IgG in the original solution.

The selectivity of the IgG precipitation was evaluated using a mixture of IgG and clarified cell culture fluid (CCF) obtained from Ambr® 250 bioreactors (Sartorius, Germany) filled with FreeStyle™ CHO cells (Thermo Fisher Scientific) grown in serum-free Gibco CHO expression media. The cells were harvested at a density of approximately 10×10^6 cells/mL. High levels of host cell proteins (HCP) were obtained by lysing the CHO cell suspension in an Isonic sonicator for an hour, with residual cells and debris removed by centrifugation. The supernatant was dialyzed against MES buffer using a D-Tube Dialyzer Maxi with molecular weight cutoff of 3.5 kDa (Merck KGaA, Germany); the dialysis was used to adjust the pH and conductivity of the solution but did not alter the concentration of the HCP due to the low molecular weight cutoff of the membrane. The powdered IgG was directly added to the dialyzed CCF. Batch precipitation was performed by the addition of $ZnCl_2$ and PEG, both with and without sodium malonate, using the same approach described previously. Feed and supernatant samples were analyzed for the HCP and DNA concentrations using CHO ELISA 3G kit (Cygnus Technologies) and Qubit™ 1× dsDNA BR, respectively.

2.3 | Filtration experiments

The critical flux associated with membrane fouling was evaluated using the flux-stepping method (Behboudi et al., 2024; Chaubal and Zydney, 2023; Minervini and

Zydney, 2022). The hollow fiber module was initially flushed with MES buffer (either with or without sodium malonate based on the composition of the IgG precipitate). The protein precipitate was then pumped from a 250 mL solution reservoir through the lumens of the hollow fiber membranes at the desired flow rate (10–50 mL/min) using a peristaltic pump (Cole-Parmer Masterflex L/S). The permeate flow rate was controlled using a second pump connected to the permeate exit port (at the far end of the module). The permeate flow rate was increased in a stepwise manner in increments of 1 mL/min every 25 min, with the feed (P_F), retentate (P_R), and permeate (P_P) pressures evaluated throughout the experiment. Filtration was continued until the gradient in the transmembrane pressure (TMP)

$$TMP = \frac{P_F + P_R}{2} - P_P, \qquad (3)$$

exceeded 0.1 kPa/min (corresponding to the onset of significant fouling).

Longer-term filtration experiments were performed using 1.5 L of precipitated IgG, collected from the tubular reactor. The hollow fiber module was again flushed with buffer, with the IgG feed and permeate flow rate set and maintained at the desired values. The TFF system was operated in total recycle mode, with the retentate and permeate both recycled back to the feed reservoir. The pressures were monitored throughout the filtration.

2.4 | Morphological and structural characterization

In-line microscopic imaging of the protein precipitate was done using a Blaze Meso probe (BlazeMetrics) placed in-line on the exit flow from the tubular precipitation reactor. More detailed characterization was performed using a DMi8 Thundered Microscope (Leica, Germany), with 3D-reconstructed images obtained by z-stacking of binarized images through the field of view.

The particle size distribution for the IgG precipitates was measured using laser diffraction (Mastersizer 3000, Malvern Panalytical, United Kingdom) with a Hydro MV wet dispersion attachment at 500 rpm. The dispersant solution within the sample tank contained 10 mM $ZnCl_2$ and 7 w/v% PEG to prevent any redissolution of the precipitated protein. The particle size distributions were calculated by the Mastersizer 3000 software (version V3.62) using Mie theory.

The properties of the precipitate were examined by differential scanning calorimetry (DSC, MicroCal VP-Capillary DSC, Malvern Panalytical, United Kingdom)

and ITC (Affinity ITC, TA Instruments, New Castle, DE). ITC was performed using IgG and $ZnCl_2$ solutions diluted 5-fold with MES buffer to maintain the heat flow within the range of the instrument. The $ZnCl_2$ was used without PEG since the PEG interfered with the analysis. The sample cell was initially filled with a 1 g/L solution of IgG in MES buffer with any added salt. The syringe was loaded with a 20 mM $ZnCl_2$ solution (in 50 mM MES along with any salts that were added to the IgG); 10 μL aliquots of the $ZnCl_2$ solution were added to the IgG every 360 s for a total of 25 injections. Baseline correction was performed using data obtained by adding $ZnCl_2$ to the MES buffer and salt solution (without IgG). Mole ratio versus enthalpy data was then fit using the Multiple Sets of Independent Binding Sites Model (Freire et al., 1990). The concentration of bound ligand is described as:

$$[L_{B,i}] = [M]\frac{n_i K_i[L]}{1 + K_i[L]}, \qquad (4)$$

where $[L_{B,i}]$ is the concentration of ligand bound to the binding sites in set i, K_i is the intrinsic site association constant, n_i is the number of binding sites of set i, and $[M]$ and $[L]$ are the concentrations of the macromolecule and free ligand, respectively. The total heat emitted or absorbed is determined by adding together the individual contributions associated with each binding site:

$$Q = V\sum_i \Delta H_i[L_{B,i}], \qquad (5)$$

where ΔH_i is the enthalpy of binding to set i.

The secondary structure of the soluble IgG in the different salt solutions was evaluated by circular dichroism spectroscopy (CD, J-1500, Jasco, MD). The IgG solution was diluted with DI water to a concentration of 0.25 mg/L and added to a 200 μL quartz cell. Three spectra were obtained for each sample using a Xenon arc lamp source, with the baseline corrected using the CD spectra obtained with the corresponding buffer. CD spectra for resolubilized IgG were obtained by adding 0.1 M glycine to the precipitate to lower the pH to 5.0; this completely reversed the binding to Zn^{2+} allowing redissolution of the protein.

3 | RESULTS AND DISCUSSION

3.1 | Precipitation yield and selectivity

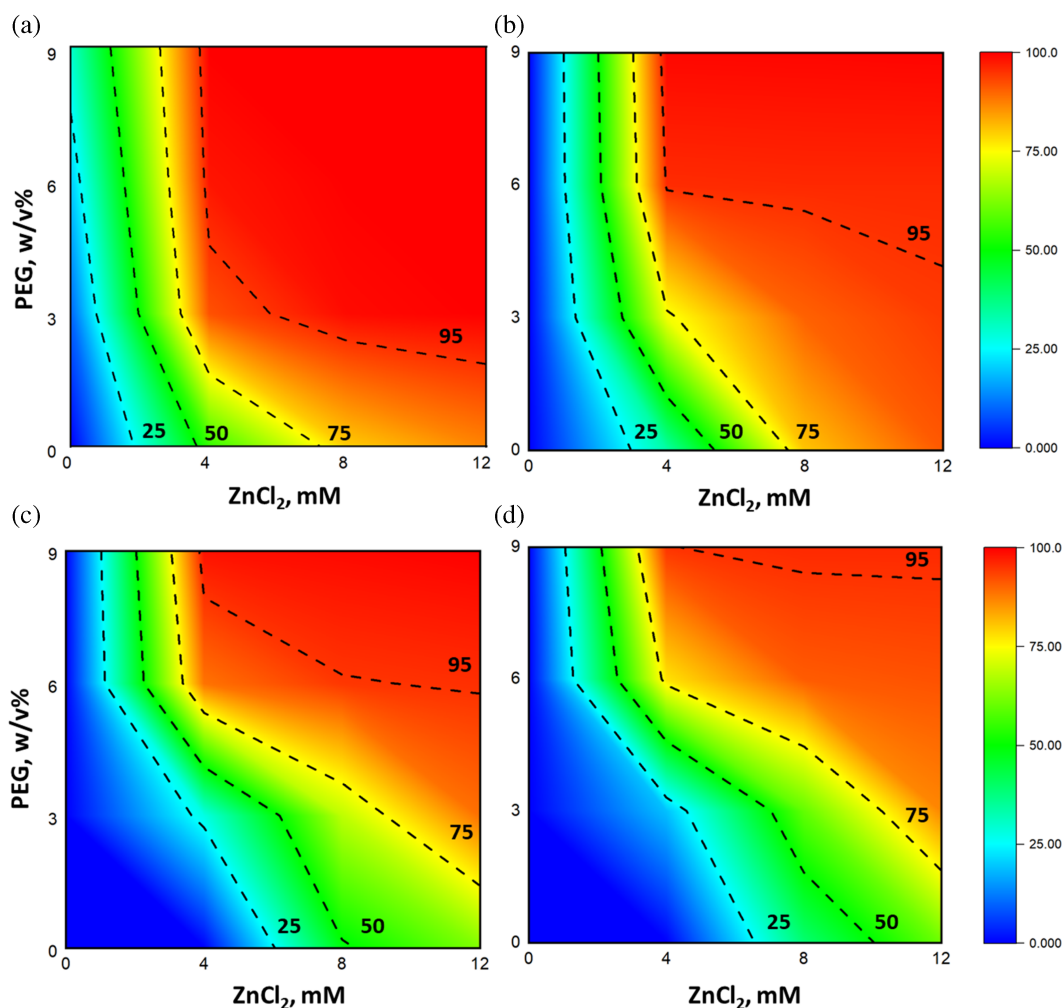Sodium malonate reduces protein solubility at high concentrations, but even 1 M sodium malonate provided

FIGURE 1 IgG yield as a function of the $ZnCl_2$ and PEG concentrations in (a) no added salt, (b) 10 mM, (c) 20 mM, and (d) 30 mM sodium malonate. IgG, immunoglobulin G; PEG, polyethylene glycol.

only 70% yield during IgG precipitation. In addition, precipitation out of sodium malonate had low selectivity. Instead, all precipitation experiments were performed with the $ZnCl_2$-PEG system that has been used previously for the precipitation of serum IgG and several different mAbs at relatively low concentrations of the two precipitants.

The addition of low concentrations of sodium malonate caused a significant reduction in the yield of the precipitated IgG from solutions containing a combination of $ZnCl_2$ and PEG. For example, IgG precipitation from a 10 mM $ZnCl_2$ solution (alone) gave an IgG yield of more than 95% in the solid phase, but this was reduced to 85% upon the addition of 10 mM sodium malonate and to below 50% in the presence of 30 mM sodium malonate. This behavior is likely due to the interaction between Zn^{2+} and the carboxylic acid groups on the malonate, which is known to chelate divalent metal cations through a bidentate structure (Deerfield et al., 1991).

Figure 1 shows contour plots (solubility "heat maps") of the precipitation yield as a function of the $ZnCl_2$ and PEG concentrations in the presence of different concentrations of sodium malonate. It was not possible to obtain >95% IgG yield in the 30 mM malonate except at very high $ZnCl_2$ and PEG. At high PEG concentrations (greater than about 6 w/v% PEG), the yield was determined almost entirely by the $ZnCl_2$ concentration. However, at lower PEG concentrations the $ZnCl_2$ and PEG act synergistically, with the addition of PEG reducing the $ZnCl_2$ concentration needed to achieve a given yield. The use of 10 mM $ZnCl_2$ and 7 w/v% PEG, the conditions employed previously by Minervini et al. (2024), provided 95% IgG yield both alone and in the presence of the 10 and 20 mM sodium malonate solutions.

The effect of sodium malonate on the selectivity of the IgG precipitation was examined using mixtures of IgG with CCF obtained from a CHO cell culture. The initial HCP concentration (after dialysis into MES) was

TABLE 1 HCP and DNA concentrations for IgG feed and precipitate.

Condition	HCP (ppm)	DNA (ppb)
Initial feed	125,000	4,000,000
Redissolved IgG (no sodium malonate)	9800	3,900,000
Redissolved IgG (20 mM sodium malonate)	9900	2,500,000

Abbreviations: HCP, host cell proteins; IgG, immunoglobulin G.

125,000 ppm as determined by the CHO ELISA. The feed also contained DNA at a concentration of 4,000,000 ppb based on the Qubit assay; the high DNA concentration is due to the lysis of the CHO cells used to provide sufficient HCP upon mixing with the IgG. Precipitation was performed from solutions containing 10 mM $ZnCl_2$ and 7 w/v% PEG in 50 mM MES buffer at pH 6.4, either with or without 20 mM sodium malonate. Results are summarized in Table 1. In both cases, the collected precipitate had HCP concentrations below 10,000 ppm, corresponding to >90% HCP removal. The precipitate formed in the absence of sodium malonate showed nearly identical levels of DNA as the feed, indicating that >95% of the DNA coprecipitated with the IgG. In contrast, the addition of 20 mM sodium malonate led to a 40% reduction in DNA content in the IgG precipitate. The lower degree of DNA precipitation in the presence of sodium malonate is likely due to chelation of the Zn.

3.2 | Morphological characterization

The structure and size of the precipitate particles were evaluated both inline, using the Blaze Meso microscopic imaging probe placed directly on the outflow from the tubular reactor, and by brightfield microscopy, with the latter performed after collection and storage of the precipitate for approximately 24 h. As shown in Figure 2, the particles formed by precipitation from the MES buffer with 10 mM $ZnCl_2$ and 7 w/v% PEG (without any added salt) had an average particle diameter of around 50 μm, consistent with laser diffraction data presented by Minervini et al. (2024). The addition of 20 mM sodium malonate caused a significant reduction in the particle size (note different z-axis scale in 3D reconstructions). The full distributions determined by laser diffraction are shown in Data S1. The smaller particles formed in the presence of sodium malonate also had a greater packing density than those formed without any added salt (16.4% vs. 11.7%); this is discussed in more detail subsequently.

Also shown for comparison are images of IgG precipitates formed in the presence of 300 mM $CaCl_2$ and 300 mM Na_2SO_4, both of which have previously been shown to give precipitates with good filterability (Minervini et al., 2024). The particles generated with 300 mM $CaCl_2$ and 300 mM Na_2SO_4 were larger than those formed in the presence of sodium malonate even though the $CaCl_2/Na_2SO_4$ concentration was 15-fold higher than that of the malonate. Note that these differences in size were not related to the amount of IgG that was precipitated from the different solutions, with the IgG yield being >95% for all conditions examined in Figure 2.

The thermal stability of the precipitated IgG was examined by differential scanning calorimetry, with results shown in Figure 3. The DSC curve for the IgG precipitated from 50 mM MES with 10 mM $ZnCl_2$ and 7 w/v% PEG (with no added salt) shows two distinct thermal transitions: $T_{m1} = 53–55°C$ and $T_{m2} = 70–73°C$. The addition of 20 mM sodium malonate caused a significant shift in the DSC curve, with T_{m1} increasing to approximately 64°C. In addition, the DSC shows clear evidence of a third transition at a temperature above 90°C.

The thermal transition temperatures for the soluble IgG and the precipitates formed in the presence and absence of sodium malonate are summarized in Table 2 along with corresponding results using 300 mM $CaCl_2$ and Na_2SO_4. Experiments were performed in triplicate with results reported as the mean ± standard deviation. The results for soluble IgG in MES buffer alone (no $ZnCl_2$ or PEG) are in good agreement with literature data (Ionescu et al., 2008); the first peak is typically associated with the Fab fragment while the second is associated with unfolding of the Fc region. The transition temperatures for the resolubilized protein (after pH adjustment) were statistically equivalent to those determined for the soluble IgG, suggesting that the precipitation had no measurable effect on the protein stability. The addition of Na_2SO_4 and sodium malonate had no significant effect on the thermal stability of the soluble IgG. In contrast, the addition of $CaCl_2$ reduced the thermal stability, with T_{m1} decreasing from 71.9 to 61.5°C. This behavior is consistent with the known effects of these salts on water structure as described by the Hofmeister series (Collins, 1997; Moelbert et al., 2004). $CaCl_2$ is commonly classified as a chaotropic (destabilizing) salt while Na_2SO_4 and sodium malonate are kosmotropic (Holyoak et al., 2003; Lawal, 2006; Yeh et al., 2010).

The transition temperatures obtained for the precipitated IgG are all well below those for the soluble protein, indicating a significant loss in stability, similar to that observed in the presence of high concentrations of urea (Nemergut et al., 2017). T_{m1} in the presence of 20 mM
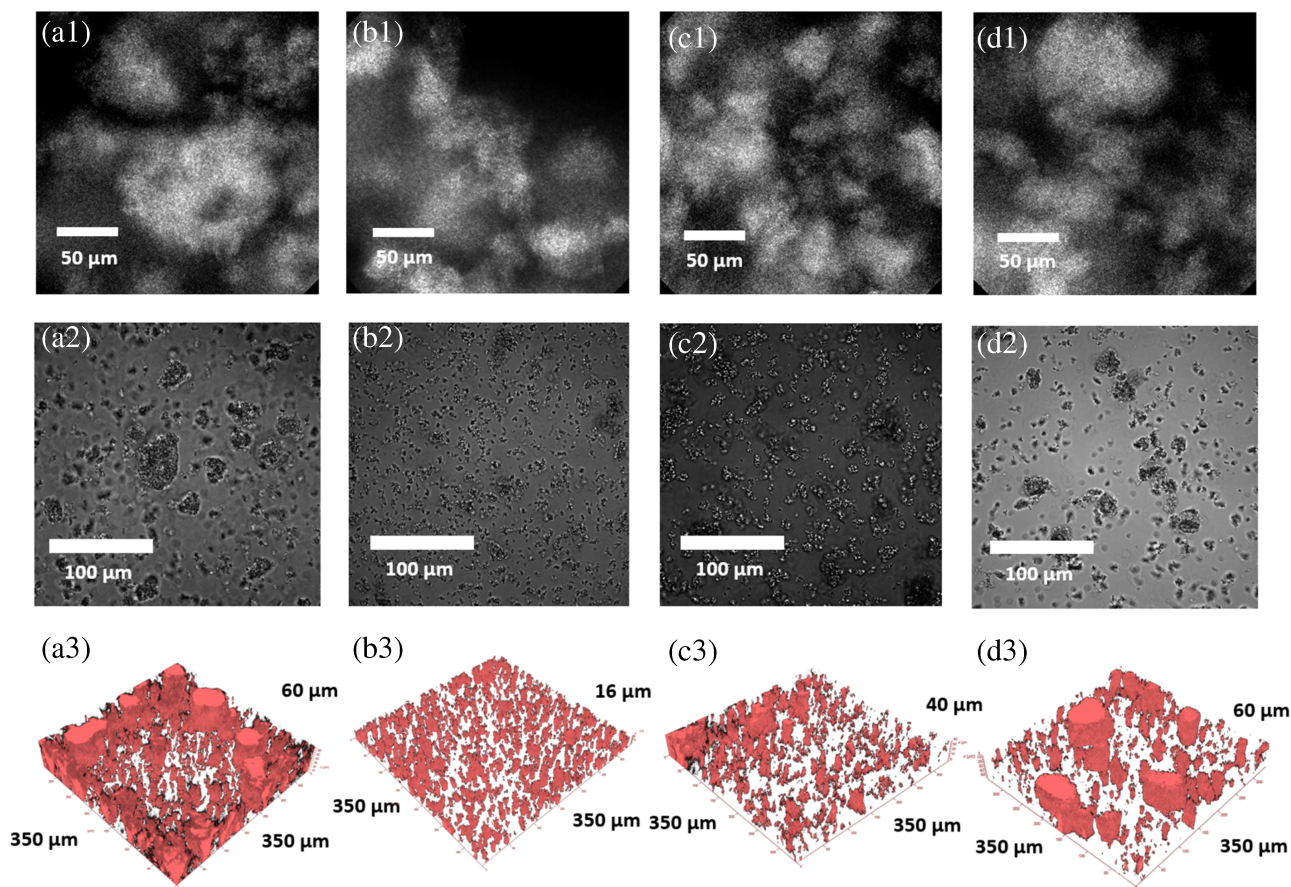
FIGURE 2 In-line microscopic images obtained from the Blaze Meso at the end of the tubular reactor (top panel), optical images after 24 h (middle panel), and 3D reconstructions based on z-stacking of optical images (bottom panel). Column a is without salt, column b is with 20 mM sodium malonate, column c is with 300 mM Na_2SO_4, and column d is with 300 mM $CaCl_2$.

FIGURE 3 DSC profiles of precipitated IgG from 50 mM PES, 10 mM $ZnCl_2$, and 7 w/v% PEG both alone and in the presence of 20 mM sodium malonate. DSC, differential scanning calorimetry; IgG, immunoglobulin G; PEG, polyethylene glycol.
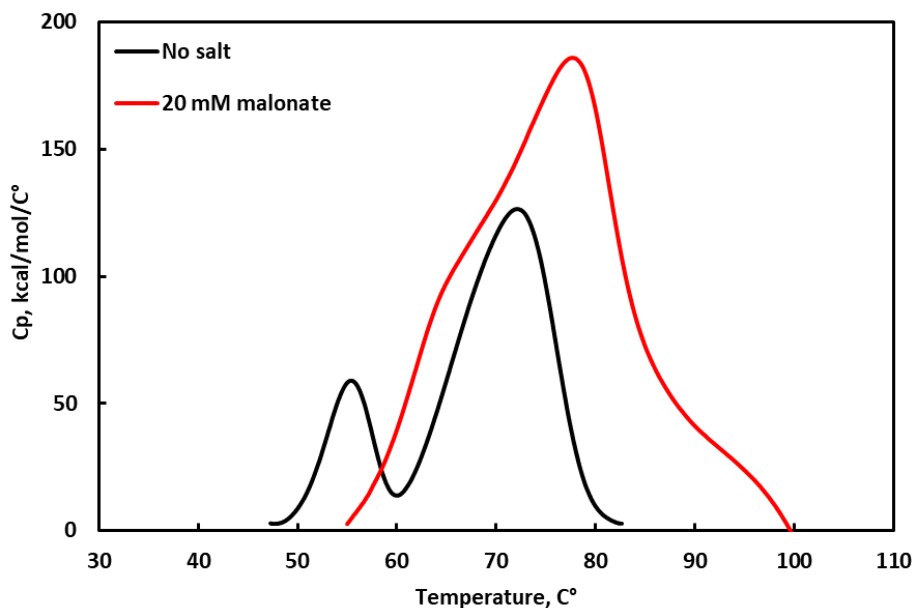
sodium malonate was significantly higher than the values in any of the other solutions, and there was also evidence of a third transition at a temperature above 90°C, which may correspond to the unfolding of a different structural domain or to a change in the intermolecular interactions stabilizing the structure of the precipitate.

TABLE 2 Thermal transition temperatures (in °C) of the soluble and precipitated IgG in different salt solutions obtained by DSC.

Soluble	T_{m1}	T_{m2}	Precipitated	T_{m1}	T_{m2}	T_{m3}
No added salt	71.9 ± 0.5	77.5 ± 0.4	No added salt	54.9 ± 0.1	72.6 ± 0.7	–
Malonate	71.6 ± 0.4	75.9 ± 0.3	Malonate	65.8 ± 0.6	78.1 ± 0.5	90.7 ± 0.4
$CaCl_2$	61.5 ± 0.1	72.4 ± 0.4	$CaCl_2$	54.1 ± 0.4	68.9 ± 0.9	–
Na_2SO_4	71.4 ± 0.8	76.5 ± 0.4	Na_2SO_4	60.5 ± 0.4	74.8 ± 0.2	–

Abbreviations: DSC, differential scanning calorimetry; IgG, immunoglobulin G.
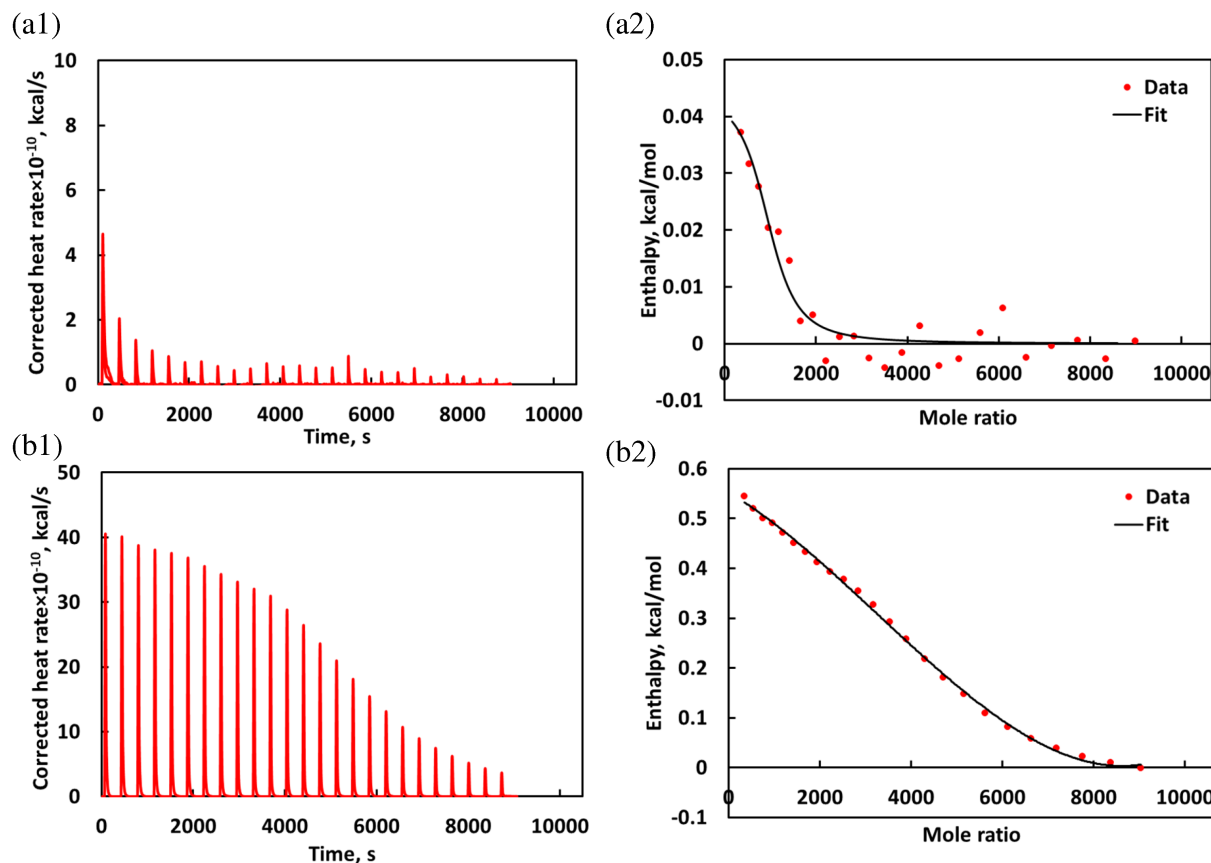

FIGURE 4 ITC thermograms of heat rate versus time (left panels) and enthalpy versus mole ratio (right panels) upon addition of $ZnCl_2$ to 1 g/L solution of IgG either (a) alone or (b) or in the presence of sodium malonate. ITC, isothermal titration calorimetry.

Further insights into the effects of sodium malonate on IgG precipitation by Zn were obtained using ITC. Data were obtained by stepwise addition of $ZnCl_2$ (in the presence or absence of sodium malonate) into a 1 g/L IgG solution with the same sodium malonate concentration as the $ZnCl_2$. As shown in Figure 4, the ITC thermograms in the absence of sodium malonate show very small heat evolution, with the maximum value of the corrected heat rate less than 2 μJ/s and decreasing to <1 μJ/s by the second injection. In contrast, the heat evolution in the presence of sodium malonate was more than 15 μJ/s for the first six injections. In both cases, the system was slightly exothermic, consistent with previous studies of protein aggregation and precipitation (Schön et al., 2017).

The interpretation of the ITC data is challenging since the Zn can not only interact directly with specific binding sites on the IgG (primarily histidine, cysteine, and various carboxylic acid side-chains), but it can also facilitate intermolecular interactions between IgG molecules that lead to IgG precipitation. Nevertheless, the integrated heat evolution data (right hand panels in Figure 4) were well-described using a simple model with n identical binding sites. The resulting thermodynamic binding parameters are summarized in Table 3. The enthalpy determined in the presence of sodium malonate (7900 cal/mol) was 180 times larger than that in the absence of sodium malonate, suggesting that the sodium malonate leads to much stronger intermolecular interactions within the IgG precipitate. This

TABLE 3 Thermodynamic parameters determined from ITC data for addition of ZnCl$_2$ to IgG in the presence of different salts.

Salt	ΔG (cal/mol)	ΔH (cal/mol)	ΔS (cal/mol/K)	K_d (mM)
None	−3800	44	13	1.44
Malonate	−740	7900	29	70.6
CaCl$_2$	−4100	42	14	1.02
Na$_2$SO$_4$	−2800	1700	15	10

Abbreviation: ITC, isothermal titration calorimetry.

TABLE 4 Structural parameters for IgG in 50 mM MES in the presence of different salts and after redissolution of the precipitated protein.

Sample	α-Helix	β-Sheet	Turn	Other
Native IgG	8.1%	34%	16%	43%
IgG (malonate)	6.1%	49%	15%	31%
IgG (CaCl$_2$)	7.1%	34%	14%	45%
IgG (Na$_2$SO$_4$)	6.5%	42%	15%	37%
Resolubilized IgG	8.1%	34%	16%	43%

Abbreviations: IgG, immunoglobulin G; MES, 2-morpholinoethanesulfonic acid.

behavior is consistent with the increased stability (and packing density) of the precipitate formed in the solution containing sodium malonate. Also shown for comparison are ITC results in the presence of CaCl$_2$ and Na$_2$SO$_4$. CaCl$_2$ had relatively little effect on either the enthalpy or entropy of the precipitation process, similar to the effect of CaCl$_2$ on the melting temperatures (Table 2). In contrast, Na$_2$SO$_4$ caused a significant increase in ΔH, although this effect is much less pronounced than that seen with sodium malonate. The calculated enthalpies are strongly correlated with the measured values of T_{m1} and T_{m2} (Table 2), suggesting that the strength of the intermolecular interactions governs the stability of the IgG precipitate.

The effect of the different salts on the structure of the soluble IgG (in the absence of Zn or PEG) was examined by CD spectroscopy with results summarized in Table 4. The native IgG has a high β-sheet content (34%). The structure of the resolubilized IgG precipitate was essentially identical to that of the native IgG, demonstrating that the Zn–PEG precipitation and additive salts cause no irreversible unfolding of the IgG. Future work with mAbs will be needed to demonstrate that the resolubilized protein maintains full biological activity. The addition of sodium malonate causes a large increase in the β-sheet content of the IgG (from 34 to 49%), corresponding to a significant increase in protein stability (Kim et al., 2016). The Na$_2$SO$_4$ also causes a significant (but smaller) increase in β-sheet content, while the CaCl$_2$ had no measurable effect on the protein secondary structure, similar to what is observed in both the ITC and DSC experiments.

3.3 | Filtration behavior

Several previous studies have shown that protein precipitates and crystals can be effectively dewatered and washed using tangential flow microfiltration (Behboudi et al., 2024; Li et al., 2019; Li et al., 2021; Minervini et al., 2023). Long-term continuous operation can be achieved by operating the TFF module below the critical flux, which is the flux at which fouling first becomes significant. A series of flux-stepping experiments were performed to measure the critical flux for precipitates formed from 5 g/L IgG solutions in 50 mM MES at pH 6.4 in the presence of 10 mM ZnCl$_2$ and 7 w/v% PEG, both alone and in the presence of different salts. The results are summarized in Figure 5, with the critical flux values plotted as a function of the packing density of the precipitate as determined from the mass of the solid pellet (Equation 2). Also shown for comparison are critical flux data obtained by Minervini et al. (2024) using the same ZnCl$_2$ and PEG system at different pH and using different buffers/salts. The data show a high degree of correlation, with the highest packing density (16.7%) and highest critical flux 90 ± 6 L/m^2/h obtained in the presence of 20 mM sodium malonate. Interestingly, the critical flux and packing densities are similar in the presence of Na$_2$SO$_4$ and CaCl$_2$ with packing densities of 14.4 and 13.5% respectively, even though the Na$_2$SO$_4$ had a significant effect on the stability of the precipitate while the CaCl$_2$ did not (as determined by DSC).

The impact of sodium malonate on the filterability of the IgG precipitate was examined further by performing a long-term filtration experiment in which 1.5 L of the IgG precipitate (formed using 10 mM ZnCl$_2$ and 7 w/v% PEG in 50 mM MES at pH 6.4), both alone and in the presence of 20 mM sodium malonate, were circulated through the hollow fiber membrane module at a feed flow rate of 30 mL/min. The filtrate flux was maintained at 143 L/m^2/h throughout the filtration, with this flux lying slightly below the critical flux for the precipitate slurry determined in the presence of 20 mM sodium malonate. These conditions correspond to 70% conversion in the module (ratio of permeate to feed flow rates of 0.7). The TMP profiles during the two
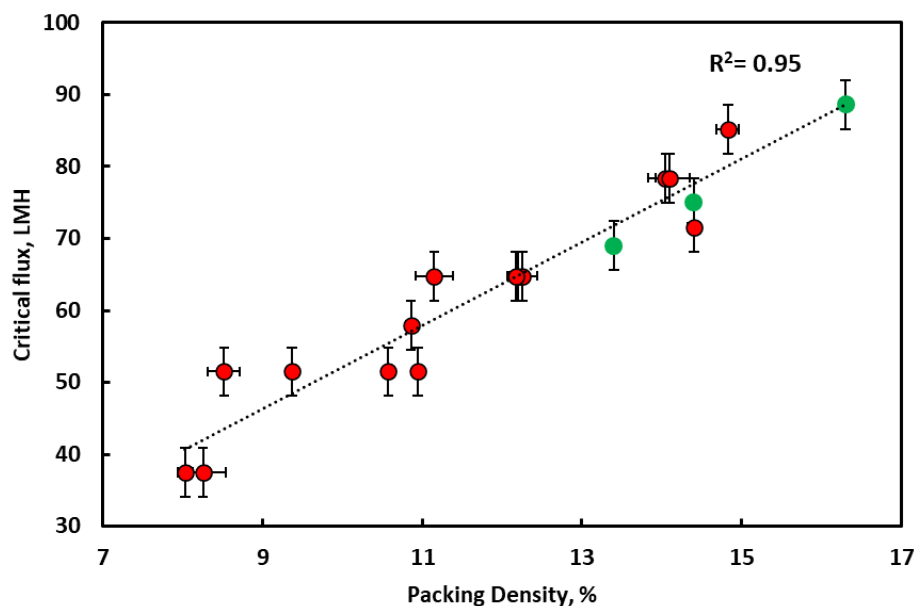
FIGURE 5 Critical flux as a function of packing density for IgG precipitates formed using 10 mM ZnCl$_2$ and 7 w/v% PEG in the presence of different salts at feed flow rate of 20 mL/min. Green circles are from this study. The red circles are from Minervini et al. (2024). IgG, immunoglobulin G; PEG, polyethylene glycol.
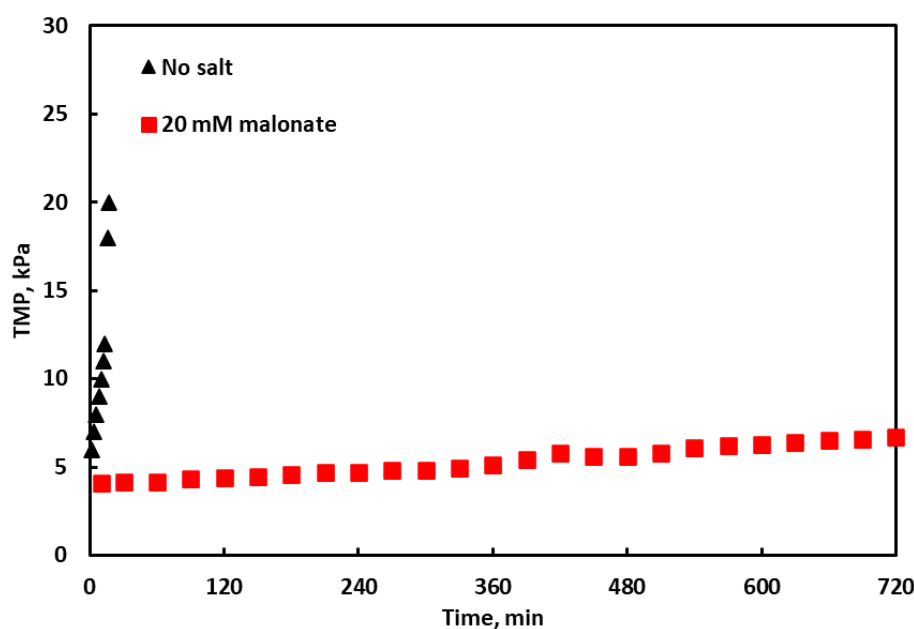

FIGURE 6 TMP profiles during constant flux filtration experiments performed using precipitated IgG (5 g/L) generated in a 50 mM MES buffer at pH 6.4 with 10 mM ZnCl$_2$ and 7 w/v% PEG both alone and in the presence of 20 mM sodium malonate. Filtration was performed at a feed flow rate of 30 mL/min and a constant filtrate flux of 143 LMH. IgG, immunoglobulin G; MES, 2-morpholinoethanesulfonic acid; PEG, polyethylene glycol; TMP, transmembrane pressure.

filtration experiments are shown in Figure 6. The TMP for the precipitate formed in the presence of 20 mM sodium malonate remained below 6.6 kPa throughout the 12 h filtration, corresponding to a TMP gradient of less than 0.0035 kPa/min. If this pressure gradient were maintained during a longer filtration, it would be possible to operate the TFF module continuously for 40 days before reaching the maximum operating TMP of 200 kPa. In contrast, the TMP for the filtration performed in the absence of the sodium malonate increased to more than 20 kPa in less than 20 min, a TMP gradient of more than 1 kPa/min.

4 | CONCLUSIONS

Although the effects of different salts on protein solubility (and precipitation) are well known, there is still very little information on how salts affect the precipitate morphology and in turn its processability. In this work, we examined the use of sodium malonate, a salt that has previously been used to enhance protein crystallizability (McPherson, 2001), to control the structure and morphology of IgG precipitates formed using a combination of ZnCl$_2$ and PEG. The addition of sodium malonate increased the β-sheet content of the soluble IgG as

determined by CD spectroscopy. This resulted in a more stable precipitate (higher T_m), consistent with the greater enthalpy of interaction evaluated from ITC measurements. There was no measurable change in IgG structure after precipitation and resolubilization (as determined by CD spectroscopy), nor was there any change in the protein stability (as determined by DSC). Future work with mAb products will be required to demonstrate that the resolubilized protein maintains its biological activity.

These changes in precipitate morphology resulted in a significantly greater packing density for the precipitate formed in the presence of sodium malonate. This may be related to the weakly attractive intermolecular interactions in sodium malonate solutions, which Dumetz et al. (2007) hypothesized as the origin of the effectiveness of sodium malonate as a crystallizing agent based on measurements of the second virial coefficient. This increase in packing density is highly correlated with an increase in the critical filtrate flux during TFF (Minervini et al., 2024), which enabled us to operate a TFF process for 12 h with minimal increase in transmembrane pressure. In contrast, the TFF membranes fouled rapidly (within 20 min) under identical conditions but for a precipitate formed in the absence of sodium malonate. Furthermore, the addition of sodium malonate improved the selectivity of the precipitation, with much less coprecipitation of DNA from a clarified CCF. Additional studies will be required to demonstrate the generalizability of this approach for improving the performance of a precipitation-filtration process for the purification of high value biopharmaceutical products, including for mAbs with different isoelectric points.

AUTHOR CONTRIBUTIONS

Ali Behboudi: Conceptualization; investigation; data curation; writing – original draft. **Mirko Minervini:** Data curation; investigation; writing – original draft. **Zachary S. Badinger:** Investigation; data curation; writing – original draft. **William W. Haddad:** Investigation; data curation; writing – original draft. **Andrew L. Zydney:** Conceptualization; funding acquisition; writing – review and editing; supervision.

ACKNOWLEDGMENTS

CONFLICT OF INTEREST STATEMENT

The authors declare no conflicts of interest.

DATA AVAILABILITY STATEMENT

Data will be made available on request.

ORCID

Andrew L. Zydney https://orcid.org/0000-0003-1865-9156

REFERENCES

Behboudi A, Minervini M, Kedzierski A, Azzariti L, Zydney AL. Tangential flow filtration for continuous processing of crystallized proteins. Sep Purif Technol. 2024;336:126311.

Burgstaller D, Jungbauer A, Satzer P. Continuous integrated antibody precipitation with two-stage tangential flow microfiltration enables constant mass flow. Biotechnol Bioeng. 2019;116(5):1053–65.

Chaubal AS, Zydney AL. Single-pass tangential flow filtration (SPTFF) of nanoparticles: achieving sustainable operation with dilute colloidal suspensions for gene therapy applications. Membranes. 2023;13(4):433.

Cohn EJ, Strong LE, Hughes WL, Mulford DJ, Ashworth JN, Melin M, et al. Preparation and properties of serum and plasma proteins. IV. A system for the separation into fractions of the protein and lipoprotein components of biological tissues and fluids. J Am Chem Soc. 1946;68(3):459–75.

Collins KD. Sticky ions in biological systems. Proc Natl Acad Sci. 1995;92(12):5553–7.

Collins KD. Charge density-dependent strength of hydration and biological structure. Biophys J. 1997;72(1):65–76.

Collins KD, Washabaugh MW. The Hofmeister effect and the behaviour of water at interfaces. Q Rev Biophys. 1985;18(4):323–422.

Deerfield DW, Fox DJ, Head-Gordon M, Hiskey RG, Pedersen LG. Interaction of calcium and magnesium ions with malonate and the role of the waters of hydration: a quantum mechanical study. J Am Chem Soc. 1991;113(6):1892–9.

Dumetz AC, Snellinger-O'Brien AM, Kaler EW, Lenhoff AM. Patterns of protein–protein interactions in salt solutions and implications for protein crystallization. Protein Sci. 2007;16(9):1867–77.

Dutra G, Komuczki D, Jungbauer A, Satzer P. Continuous capture of recombinant antibodies by $ZnCl_2$ precipitation without polyethylene glycol. Eng Life Sci. 2020;20(7):265–74.

Ferreira-Faria D, Domingos-Moreira F, Aires-Barros MR, Ferreira A, Azevedo AM. Continuous precipitation of antibodies using oscillatory flow reactor: a proof of concept. Sep Purif Technol. 2023;317:123924.

Foster PR, Dickson AJ, Stenhouse A, Walker EP. A process control system for the fractional precipitation of human plasma proteins. J Chem Technol Biotechnol. 1986;36(10):461–6.

Freire E, Mayorga OL, Straume M. Isothermal titration calorimetry. Anal Chem. 1990;62(18):950A–959A.

Holyoak T, Fenn TD, Wilson MA, Moulin AG, Ringe D, Petsko GA. Malonate: a versatile cryoprotectant and stabilizing solution for salt-grown macromolecular crystals. Acta Crystallogr Sect D. 2003;59(12):2356–8.

Ionescu RM, Vlasak J, Price C, Kirchmeier M. Contribution of variable domains to the stability of humanized IgG1 monoclonal antibodies. J Pharm Sci. 2008;97(4):1414–26.

Kaushik JK, Bhat R. A mechanistic analysis of the increase in the thermal stability of proteins in aqueous carboxylic acid salt solutions. Protein Sci. 1999;8(1):222–33.

Kim DN, Jacobs TM, Kuhlman B. Boosting protein stability with the computational design of β-sheet surfaces. Protein Sci. 2016; 25(3):702–10.

Lawal OS. Kosmotropes and chaotropes as they affect functionality of a protein isolate. Food Chem. 2006;95(1):101–7.

Li Z, Chen T-H, Andini E, Coffman JL, Przybycien T, Zydney AL. Enhanced filtration performance using feed-and-bleed configuration for purification of antibody precipitates. Biotechnol Prog. 2021;37(1):e3082.

Li Z, Gu Q, Coffman JL, Przybycien T, Zydney AL. Continuous precipitation for monoclonal antibody capture using countercurrent washing by microfiltration. Biotechnol Prog. 2019;35(6): e2886.

Liang K, Luo H, Li Q. Enhancing and stabilizing monoclonal antibody production by Chinese hamster ovary (CHO) cells with optimized perfusion culture strategies. Front Bioeng Biotechnol. 2023;11:1112349.

McPherson A. A comparison of salts for the crystallization of macromolecules. Protein Sci. 2001;10(2):418–22.

Melander W, Horváth C. Salt effects on hydrophobic interactions in precipitation and chromatography of proteins: an interpretation of the lyotropic series. Arch Biochem Biophys. 1977;183(1): 200–15.

Minervini M, Behboudi A, Marzella JR, Zydney AL. Optimizing particle morphology during antibody precipitation for enhanced tangential flow filtration performance. Sep Purif Technol. 2024;338:126574.

Minervini M, Mergy M, Zhu Y, Gutierrez Diaz MA, Pointer C, Shinkazh O, et al. Continuous precipitation-filtration process for initial capture of a monoclonal antibody product using a four-stage countercurrent hollow fiber membrane washing step. Biotechnol Bioeng. 2023. https://doi.org/10.1002/bit.28525 Online ahead of print.

Minervini M, Zydney AL. Effect of module geometry on the sustainable flux during microfiltration of precipitated IgG. J Membr Sci. 2022;660:120834.

Moelbert S, Normand B, De Los RP. Kosmotropes and chaotropes: modelling preferential exclusion, binding and aggregate stability. Biophys Chem. 2004;112(1):45–57.

Nemergut M, Žoldák G, Schaefer JV, Kast F, Miškovský P, Plückthun A, et al. Analysis of IgG kinetic stability by differential scanning calorimetry, probe fluorescence and light scattering. Protein Sci. 2017;26(11):2229–39.

Pons Royo MC, De Santis T, Komuczki D, Satzer P, Jungbauer A. Continuous precipitation of antibodies by feeding of solid polyethylene glycol. Sep Purif Technol. 2023;304:122373.

Recanati G, Lali N, Mathia FD, Jungbauer A. Residence time distribution of continuous capture of recombinant antibody by precipitation and two stage tangential flow filtration. J Chem Technol Biotechnol. 2024;99(5):1201–11.

Recanati G, Pappenreiter M, Gstoettner C, Scheidl P, Vega ED, Sissolak B, et al. Integration of a perfusion reactor and continuous precipitation in an entirely membrane-based process for antibody capture. Eng Life Sci. 2023;23(10):e2300219.

Schön A, Clarkson BR, Jaime M, Freire E. Temperature stability of proteins: analysis of irreversible denaturation using isothermal calorimetry. Proteins Struct Funct Bioinf. 2017;85(11):2009–16.

Shih Y-C, Prausnitz JM, Blanch HW. Some characteristics of protein precipitation by salts. Biotechnol Bioeng. 1992;40(10): 1155–64.

Shukla AA, Wolfe LS, Mostafa SS, Norman C. Evolving trends in mAb production processes. Bioeng Transl Med. 2017;2(1):58–69.

Yeh V, Broering JM, Romanyuk A, Chen B, Chernoff YO, Bommarius AS. The Hofmeister effect on amyloid formation using yeast prion protein. Protein Sci. 2010;19(1):47–56.

SUPPORTING INFORMATION

Additional supporting information can be found online in the Supporting Information section at the end of this article.